arXiv:1701.01526v1 [astro-ph.SR] 6 Jan 2017

Magnetic separatrix as the source region of the plasma supply for an active-region filament

P. Zou[1,2,3], C. Fang[1,2,3], P. F. Chen[1,2,3], K. Yang[1,2,3], & Wenda Cao[4]

Received _____; accepted _____

[1]School of Astronomy & Space Science, Nanjing University, Nanjing 210023, China

[2]Key Lab of Modern Astronomy & Astrophysics (Nanjing University), Ministry of Education, Nanjing 210023, China

[3]Collaborative Innovation Center of Modern Astronomy and Space Exploration, Nanjing 210023, China

[4]Big Bear Solar Observatory, New Jersey Institute of Technology, 40386 North Shore Lane, Big Bear City, CA 92314, USA

ABSTRACT

Solar filaments can be formed via chromospheric evaporation followed by condensation in the corona or by the direct injection of cool plasma from the chromosphere to the corona. In this paper, with high-resolution Hα data observed by the 1.6 m New Solar Telescope of the Big Bear Solar Observatory on 2015 August 21, we confirmed that an active-region filament is maintained by the continuous injection of cold chromospheric plasma. We find that the filament is rooted along a bright ridge in Hα, which corresponds to the intersection of a magnetic quasi-separatrix layer with the solar surface. This bright ridge consists of many small patches and the sizes of these patches are comparable to the width of the filament threads. It is found that upflows originate from the brighter patches of the ridge, whereas the downflows move toward the weaker patches of the ridge. The whole filament is composed of two opposite directional streams, implying that longitudinal oscillations are not the only cause of the counterstreamings, and unidirectional siphon flows with alternative directions are another possibility.

Subject headings: Sun: filaments, prominences, Sun: chromosphere, Sun: magnetic fields

1. Introduction

Solar filaments are elongated dark structures appearing on the solar disk typically observed in Hα (Parenti 2014; Vial & Engvold 2015). They show similar, but more extended, dark features in extreme ultraviolet (EUV) lines or continuum (Heinzel et al. 2001; Schmieder et al. 2004). When they are seen above the solar limb they are called prominences, it is revealed that filaments are dense clouds suspended in the corona. While their temperature is ∼100 times smaller than that of the surrounding corona, their density is ∼100 times higher than the latter, leading to the total mass of a filament in the range of 10^{14}–10^{15} g (Labrosse et al. 2010). The mass is so high that the mass of several quiescent filaments is comparable with the whole mass of the corona (Malherbe 1989). In other words, the mass of a filament cannot be supplied by the condensation of the local corona itself (Mackay et al. 2010). Therefore, the filament material must originate from the chromosphere.

Several mechanisms have been proposed to explain how the chromosphere supplies the necessary mass into the supporting magnetic structure in the corona, either a flux rope or a sheared arcade. One popular mechanism is the evaporation-condensation model (Poland & Mariska 1986), i.e., chromospheric plasmas are heated up to the coronal temperature and then evaporated into the corona along the magnetic field line. As the hot plasma accumulates, the coronal loop finally becomes so dense that the criterion for thermal instability is satisfied, and the coronal plasma cools down to $\sim 10^4$ K in a catastrophic way (Park 1953). This model can explain the sudden appearance of many filaments, as illustrated by radiative hydrodynamic or hydromagnetic simulations in one dimension (Karpen et al. 2001), two dimensions (Xia et al. 2012), and even three dimensions (Xia & Keppens 2016). The multiwavelength observations in EUV confirmed the cooling process from ∼1.5 MK all the way to 30,000 K in ∼8 hr (Liu et al. 2012). Alternatively,

the cold chromospheric material can be directly injected into the corona along the magnetic field lines, as observed by Wang (2001) and Chae (2003). The injection may result from magnetic reconnection in the low atmosphere as magnetic elements with the minority polarity approach the dominant polarity (Wang 2001). This model is also supported by accumulating observational evidence, which shows that the endpoints of a filament or its barbs correspond to mixed magnetic polarities, and cold jets flow toward the filament spine (Zou et al. 2016). It is noted, however, that the mixed polarities are not the only place where magnetic reconnection can happen. A more general case would be the magnetic quasi-separatrix layers (QSLs), where current sheets can be formed easily and reconnection can happen even when a single polarity is present on the photospheric magnetogram. In this *Letter*, with the combined high-resolution observations of the *Solar Dynamics Observatory* (*SDO*) and the 1.6 m New Solar Telescope (NST, Cao et al. 2010; Goode & Cao 2012), at Big Bear Solar Observatory (BBSO), we report that the thread clusters of an active-region filament are rooted along a bright ridge in Hα, which corresponds to the intersection of a magnetic QSL with the solar surface. The observations are described in §2, and the results are presented in §3, which are followed by discussions in §4.

2. Observations and Data Analysis

A small filament is located in the active region NOAA 12403 (S27E24) on 2015 August 21, as shown by Figure 1(a), which is the Hα image from the Global Oscillation Network Group (GONG, Harvey et al. 2011). This filament was observed by the BBSO/NST from 17:00 UT to 19:00 UT. Its field of view (FOV) covers only the western half of the filament, as indicated by the yellow box in Figure 1(b). The *Interface Region Imaging Spectrograph* (*IRIS*; De Pontieu et al. 2014) mission observed the eastern half of the filament, with both imaging in a wider FOV and spectroscopy in a smaller FOV as indicated by the blue solid

and dashed boxes in Figure 1(b).

For observing the fine structures of the filament, the Visible Image Spectrometer (VIS) onboard NST, which uses a Fabry-Pérot etalon with the bandpass of 0.07 Å, is required. It provides the Hα line-center, ±0.2 Å, ±0.4 Å, ±0.6 Å, ±0.8 Å, and ±1.0 Å filtergrams. The FOV is about 70″ × 70″ and the image resolution is 0.″030 per pixel and the cadence is 32 s. The photospheric motions can be observed by the Broad Filter Imager (BFI) which uses a TiO filter (7057 Å) with a bandpass of 10 Å. Its spatial resolution is 0.″034 per pixel and the cadence is 15 s.

The Mg II and Si IV spectra observed by *IRIS* are used for spectral diagnostics of the filament. Its raster width is 0.″35 and the spectral resolution is 0.051 Å per pixel for Mg II line and 0.025 Å per pixel for Si IV respectively. *IRIS* provides the slit-jaw images of near ultraviolet emission (2796 Å and 2832 Å) with the bandpass of 4 Å and Far Ultraviolet emission (1330 Å and 1400 Å) with the bandpass of 40 Å. Both the slit-jaw images have a pixel size of 0.″33.

In order to understand the magnetic environment and the underlying mechanism of the filament activity, we use the magnetograms observed by the Helioseismic and Magnetic Imager (HMI, Scherrer et al. 2012; Schou et al. 2012) on board the *Solar Dynamics Observatory SDO*. The magnetograms have a resolution of 0.″60 per pixel and a cadence of 45 s. Furthermore, magnetic extrapolation can help us determine more detail about the magnetic configuration. Data from the Space-weather HMI Active Region Patches (SHARPs, Bobra et al. 2014) are used. The SHARPs data have resolved the 180° ambiguity by adopting the minimum energy method (Metcalf 1994; Metcalf et al. 2006). The coordinate system has been modified by the Lambert method (Bobra et al. 2014), and the project effects are corrected with the method described by Gary & Hagyard (1990). In order to coalign the observed data from different telescopes, both the BBSO/NST Hα line

wing images and the slit-jaw images are compared with the continuum images observed by *SDO*/HMI.

3. Results

Figure 2(a) displays a single snapshot of the Hα images at line center. It is clear that the filament is composed of many thin threads, terminating at the western endpoints of the filament. The attached animation shows that these threads are highly dynamic. New threads are formed continuously, and then move along the direction of the threads. A clear impression is that the upper part of the filament is dominated by rightward-moving threads, which drain down to the solar surface, whereas the lower part of the filament is associated with leftward-moving threads, which originate from the western endpoints of the filament. In order to see the dynamics more clearly, we select two slices, i.e., yellow and blue slices, along the upper half and the lower half of the filament, respectively, as marked in Figure 2(a). For both slices, the starting points are chosen to be the western endpoint of the filament. The time evolution of the intensity along the yellow and blue slices are plotted in panels (b) and (c) of Figure 2, respectively. In order to show the flows clearly, the image of the Hα line wing is used. It is seen that along the yellow slice, most of the intensity patterns show a motion toward the starting point of the slice, as indicated by dashed lines in Figure 2(b). In contrast, the blue slice is associated with sporadic ejections moving away from the starting point, as indicated by dashed lines in Figure 2(c). According to the time-distance diagrams, we find that these flows are sporadic, with an interval of $\sim$20 min. Each time, the flow lasts for about 10 min.

It is noted in Figure 3(a) that all of the threads are rooted along a bright ridge in Hα. The ridge is not uniform in brightness, with some parts fainter than others. Interestingly, the yellow slice corresponds to the threads rooted at the fainter part of the

ridge, whereas the blue slice corresponds to the threads mapped to the brighter part. In order to understand the magnetic properties of this bright ridge, we superpose the Hα intensity contour lines of its brightest kernels on the *SDO*/HMI magnetogram in Figure 3(c). Apparently the bright ridge in Hα extends from the eastern edge of a positive sunspot all the way down to a region close to the magnetic polarity inversion line (PIL) between a negative polarity and a positive polarity further south. It is noted that the bright kernels have typical sizes of $0\farcs1 \sim 0\farcs2$, which are comparable to the width of the filament threads. These fine structures can only be seen in high-resolution observations.

With the *SDO*/HMI SHARPS vector magnetograms, we extrapolate the nonlinear force-free coronal magnetic field by applying the optimization method (Wiegelmann 2004). Once the 3-dimensional coronal magnetic field is obtained, its topological parameters, e.g., the squashing factor Q (Titov et al. 2002), can be calculated. As discussed by Demoulin (2006), the locations with extremely large Q correspond to QSLs, across which the magnetic connectivity changes drastically. The distribution of Q in the solar surface is plotted in Figure 3(d). Comparing panels (a) and (d), it is seen that the bright ridge in Hα is associated with large Q, meaning that the Hα bright ridge corresponds to the footpoint of a QSL.

The left panel of Figure 4 displays the *IRIS* slit-jaw image in Mg II k 2796 Å which covers the eastern part of the filament. Because of its wide bandpass, the filament is nearly invisible. Even though, it is seen that the eastern endpoints of the filament are also rooted at an area with continuing brightenings. A narrow region with $-457'' \leq x \leq -448''$ is measured by the *IRIS* spectrometer with the scanning mode. It takes ∼200 s to complete one raster. Panels (b) and (c) in Figure 4 display the Dopplergrams at two times separated by ∼1 hr. It is seen that blue shifts persist around the position (-456″, -345″) as indicated by the blue arrows, whereas red shifts persist around the position (-448″, -345″) as indicated

by the red arrows. The blue shifts, i.e., upflows, have typical velocities of $\sim$ 5 km s^{-1}, and the red shifts, i.e., downflows, have typical velocities of $\sim$ 10 km s^{-1}.

The non-linear force free field (NLFFF) extrapolation of the filament magnetic configuration is given in Figure 5. On comparing with the magnetic field lines in Figure 5 with Figure 4, it is revealed that the blue-shifted area is roughly cospatial with the pink field lines which are mapped to the yellow dashed line marked in Figure 2(a), whereas the red-shifted area is associated with the yellow field lines which are mapped to the blue dashed line in Figure 2(a). The Doppler shift pattern is consistent with the extrapolated magnetic connectivity, i.e., cold upflows are ejected at the eastern footpoints of the pink field lines in Figure 5, and then move westward until draining down to the western footpoint of the pink field lines. In contrast, another stream of cold upflows is ejected at the western footpoints of the yellow field lines, and then move eastward until draining down to the eastern footpoints of the yellow field lines.

4. Discussions

It is well known that filament material should originate from the chromosphere. However, it has been debated whether the cold chromospheric material is ejected into the corona directly as claimed by the injection model (Chae 2003), or is heated up to $\sim$2 MK and evaporated to the corona where thermal instability leads to catastrophic cooling to $\sim 10^4$ K, as claimed by the evaporation-condensation model (Poland & Mariska 1986). With the solid observations showing both direct injection (Zou et al. 2016) and in-situ formation via thermal instability (Liu et al. 2012), it seems that both mechanisms are at work in the solar corona.

For the injection model, it has been proposed that the injected upflows are cold

jets resulting from the magnetic reconnection in the solar lower atmosphere (Wang 1999; Chae 2003). One unclear issue regarding this model is how reconnection can drive cool material to a height of ∼100 Mm in the corona without heating the plasma too much (Mackay et al. 2010). According to Jiang et al. (2012), when the reconnection point is located in the low chromosphere, most of the released magnetic energy goes to the kinetic energy of the reconnection outflow, and the plasma is heated weakly. Furthermore, radiation and ionization consume a significant part of the thermal energy (Chen et al. 2001). These numerical simulations indicate that it is possible to have fast but cold jets from the chromosphere to the corona. For the evaporation-condensation model, however, the upper chromospheric plasma should be heated. Although in most numerical models (Karpen et al. 2001; Xia et al. 2012; Xia & Keppens 2016), a localized heating is specified in the chromosphere without mentioning which mechanism, it is perceivable that the heating is also due to magnetic reconnection. This means that both of the models for the filament formation require magnetic reconnection in the chromosphere, and canceling magnetic features have been discovered to be associated with the mass supply for filaments (Wang 2001; Chae 2003; Zou et al. 2016). With this *Letter*, we emphasize that the mixed polarities are not the only place which can host chromospheric magnetic reconnection and inject cold plasma to feed a filament. A more general scenario for the reconnection to happen is the magnetic QSL. At least for the active-region filament observed on 2015 August 21, its endpoint is found to be rooted at a magnetic QSL, which is calculated from the extrapolated magnetic field and manifested by a bright ridge in Hα. Our high-resolution observation reveals that the bright ridge consists of many small kernels with sizes comparable to the width of the filament threads. It implies that the mass supply of the filament threads may come from the bright kernels.

Different formation mechanisms of solar filaments require different magnetic configurations. For the filaments described by the evaporation-condensation model, a

magnetic dip is necessary for a flux tube, otherwise the condensed plasma can not be suspended in the corona, and would drain down to the solar surface along the field line upon formation. However, for the filaments formed via continuous chromospheric injection, they are maintained dynamically with quasi-continuous siphon flows as demonstrated by Wang (1999) and the observations in this paper. In this case, magnetic dips are not necessary. They may or may not exist in the solar corona. It seems that this kind of dynamically-sustained filaments may be of quiescent type (Wang 1999) or of active-region type (this paper).

A typical dynamic feature found in solar filaments is the counterstreaming (Zirker et al. 1998). Their nature has not yet been fully understood. In our viewpoint, the nature of counterstreamings is not independent of the formation mechanism and the magnetic configuration. In the case of the evaporation-condensation model, the counterstreamings are probably due to the longitudinal oscillation of the filament threads (Luna et al. 2014), where a magnetic dip exists near the top of the magnetic field line. In the case of the chromospheric injection model, no longitudinal oscillations are needed, nor are the magnetic dips. In this case, the counterstreamings are the combination of unidirectional flows as implied by the spectroscopic observations (Chen et al. 2014). In this paper, the high-resolution Hα observations clearly support such a scenario, as revealed by Figure 2. It seems that the streaming is like a siphon flow, moving from the brighter (hence with higher pressure) footpoint to the weaker (hence with lower pressure) footpoint. As seen from Figure 2, the counterstreaming pattern of this filament is very simple, with the upper half strand moving westward and the lower half strand moving eastward.

The authors are grateful to the referee for the detailed suggestions. This work was supported by the National Natural Science Foundation of China (NSFC) under the grant numbers 11533005, 11025314, and 13001003 as well as NKBRSF under grant 2014CB744203.

P.F.C. was also supported by Jiangsu 333 Project. W.C. acknowledges the support of the US NSF (AGS-0847126 and AGS-1250818) and NASA (NNX13AG14G). This work was also supported by the project "The Strategic Priority Research Program of the Chinese Academy of Sciences" (XDB09000000).

REFERENCES

Bobra, M. G., Sun, X., Hoeksema, J. T., et al. 2014, Sol. Phys., 289, 3549

Cao, W., Gorceix, N., Coulter, R., et al. 2010, AN, 331, 636

Chae, J. 2003, ApJ, 584, 1084

Chen, P. F., Fang, C., & Ding, M.-D., ChJAA, 1, 176

Chen, P. F., Harra, L. K., & Fang, C. 2014, ApJ, 784, 50

De Pontieu, B., Title, A. M., Lemen, J. R., et al. 2014, Sol. Phys., 289, 2733D

Demoulin, P., 2006, Advance in Space Research, 37, 1269

Gary, G. A., & Hagyard, M. J. 1990, Sol. Phys., 126, 21

Goode, P. R., & Cao, W. 2012, Proc. SPIE, 8444, 3

Harvey, J. W., Bolding, J., Clark, R., et al., 2011, Bulletin of the American Astronomical Society, 1745

Heinzel, P., Schmieder, B., & Tziotziou, K., 2001, ApJ, 561, 223

Jiang, R.-L., Fang, C., & Chen, P. F., 2012, ApJ, 751, 152

Karpen, J. T., Antiochos, S. K., Hohensee, M., et al. 2001, ApJ, 553, L85

Labrosse, N., Heinzel, P., Vial, J. C., et al. 2010, Space Science Review, 151, 243

Liu, W., Berger, T. E., & Low, B. C., 2012, ApJ, 745, 21L

Luna, M., Knizhnik, K., Magluch, K, et al., 2014, ApJ, 785, 79L

Mackay, D. H., Karpen, J. T., Ballester, J. L., Schmieder, B., & Aulanier, G., 2010, Space Science Review, 151, 333

Malherbe, J. M., 1989, In: Astrophysics and Space Science Library, Vol. 150, Dynamics and structure of quiescent solar prominences, ed. E. R. Priest, 115-141

Metcalf, T. R. 1994, Sol. Phys., 155, 235

Metcalf, T. R., Leka, K. D., Barnes, G., et al. 2006, Sol. Phys., 235, 161

Parenti, S., 2014, LRSR, 11, 1

Park, E. N., 1953, ApJ, 117, 431

Poland, A. I., & Mariska, J. T., 1986, Sol. Phys., 104, 303

Scherrer, P. H., Schou, J., Bush, R. I., et al. 2012, Sol. Phys., 275, 207

Schmieder, B., Mein, N., Deng, Y., et al. 2004, Sol. Phys., 223, 119

Schou, J., Scherrer, P. H., Bush, R. I., et al. 2012, Sol. Phys., 275, 229

Titov, V. S., Horning, G. & Demoulin, P., 2002, JGR, 107, 1164

Vial, J.-C., & Engvold, O. (ed.) 2015, in Astro-physics and Space Science Library 415, Solar Prominences (Berlin: Springer)

Wang, Y.-M., 1999, ApJ, 520, 71

Wang, Y.-M., 2001, ApJ, 560, 456

Wiegelmann, T. 2004, Sol. Phys., 219, 87

Xia, C., Chen, P. F., & Keppens, R., 2012, ApJ, 782, 26L

Xia, C., & Keppens, R., 2016, ApJ, 823, 22

Zirker, J. B., Engvold, O., & Martin, S. F., 1998, Nature, 396, 440

Zou, P., Fang, C., Chen, P. F., et al. 2016, ApJ, 831, 123

This manuscript was prepared with the AAS LaTeX macros v5.2.

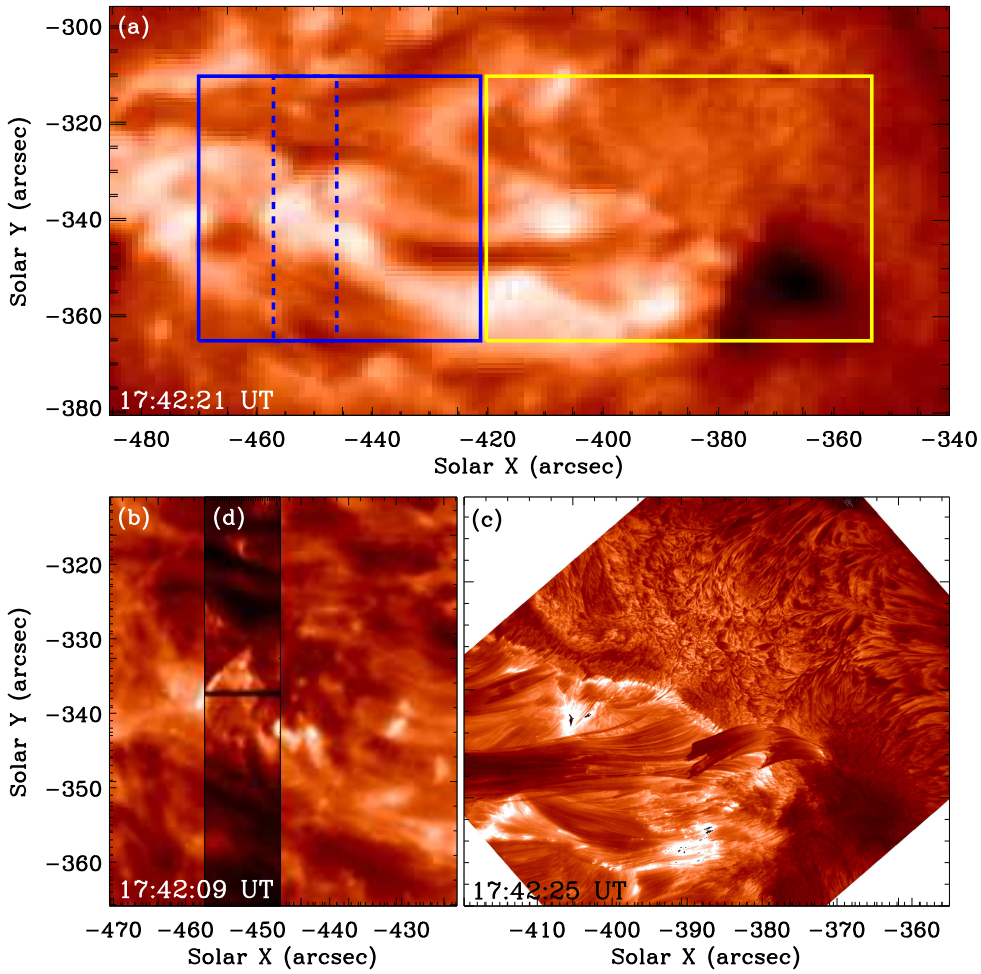

Fig. 1.— The filament cannot be observed in Hα images before our observation period (panel (a)). Panel (b) gives the position of the filament. The FOV of each instrument is also shown. The FOV of NST covers the west half of the filament (panel (d)) and that of the *IRIS* covers the other half (panel (c)). The scanning region can observe one endpoint of the filament (panel (e)).

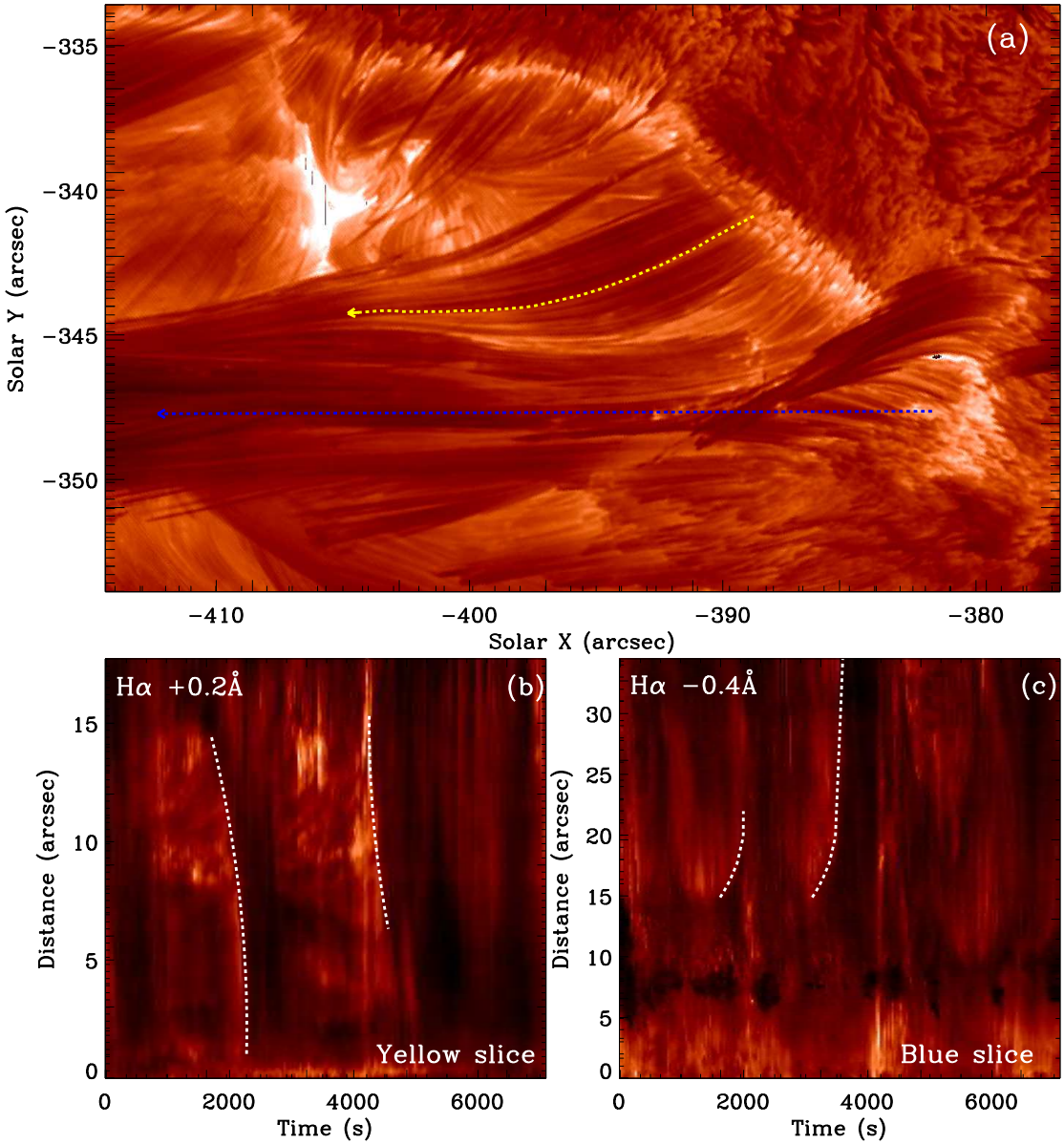

Fig. 2.— Positions of the yellow and blue slices (top panel) and time-distance plots of the yellow slice (panel (b)) and that of the blue slice (Panel (c)). The attached animation also shows the dynamic motion of filament threads.

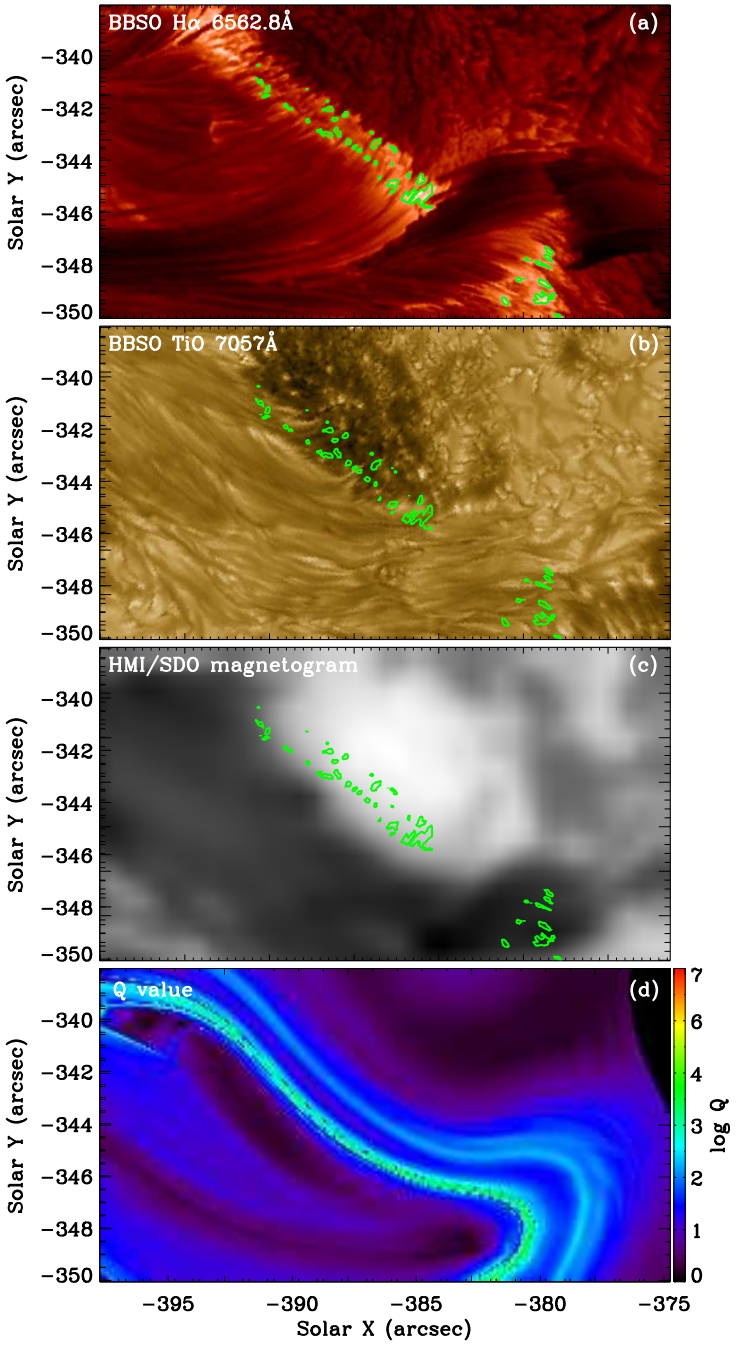

Fig. 3.— Contours of bright patches on the Hα line center image (panel (a)), the photospheric TiO line image (panel (b)), and the magnetogram (panel (c)). The bottom panel shows the Q values of this area.

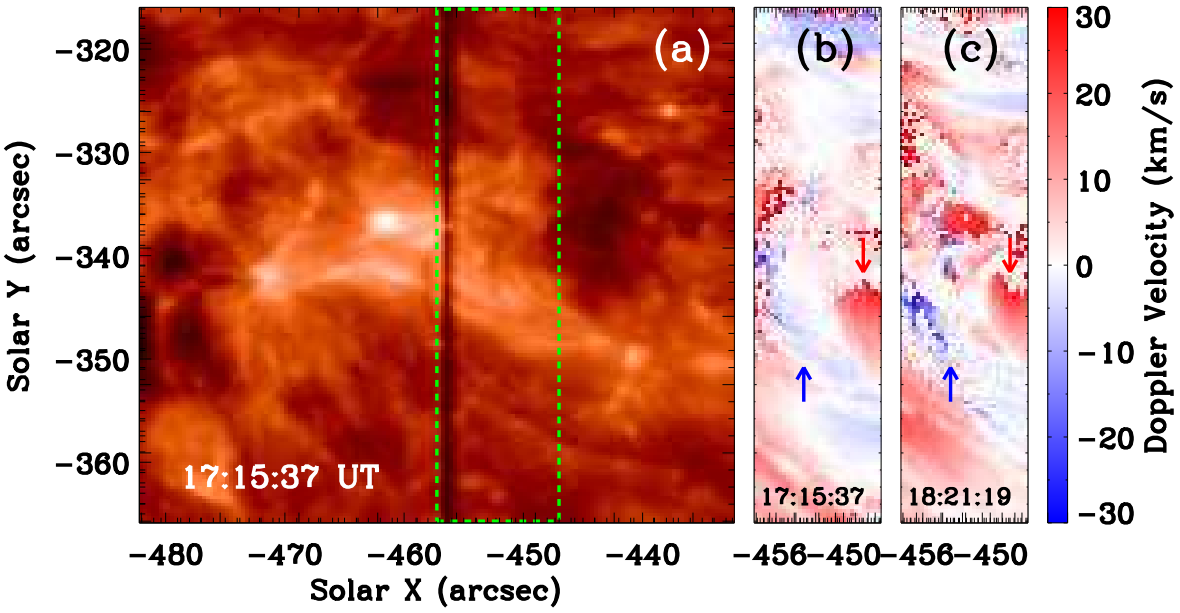

Fig. 4.— Slit-jaw image of the Mg II line and the scanning region (green-dashed box) (panel (a)). The Dopplergrams of the scanning region at different times are shown in panels (b) and (c). The blue and red arrows on each Dopplergram indicate the blue-shifted part and the red-shifted part respectively.

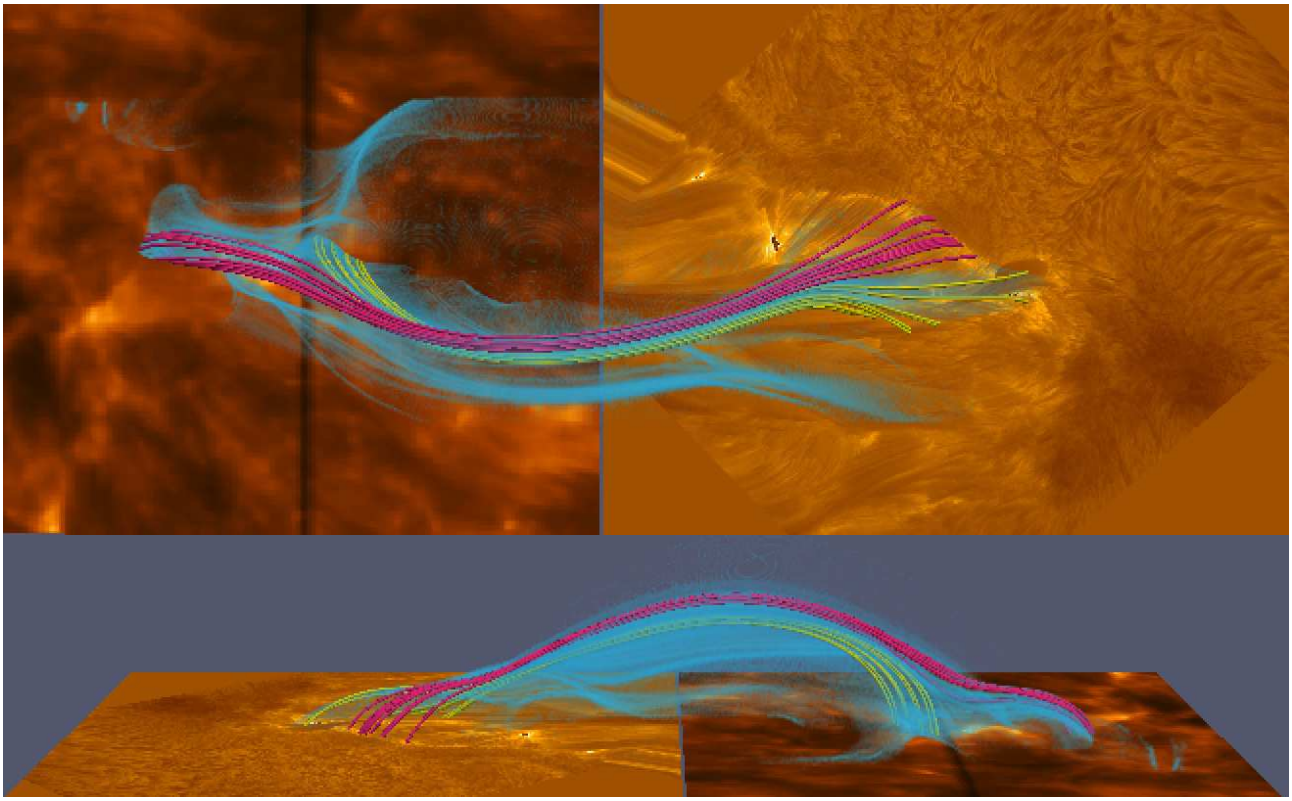

Fig. 5.— Vertical (upper panel) and horizontal view (lower penal) of the filament magnetic configuration. The pink and yellow magnetic lines correspond to different parts of the filament which have opposite directional flows. The distribution of Q value is also shown by the cyan fog. The displayed Q values are larger than 10^3.